Rapid response optical RIGT, and relative determination of $T - T_{90}$ across $(293 < T < 433)$ K

Patrick Egan[a)]

National Institute of Standards and Technology, 100 Bureau Drive, Gaithersburg, MD 20899, USA

(Dated: 16 August 2023)

Abstract. A refractive-index gas thermometer has been used to determine $T - T_{90}$ in the temperature range $(293 < T < 433)$ K within about 3 µK/K relative standard uncertainty. The thermometer is based on an optical resonator operating at 633 nm wavelength. The working principle first measured helium refractivity at known pressure and temperature to determine the temperature-dependent compressibility of the resonator. With accurate knowledge of compressibility, the resonator was then run in argon to determine $T - T_{90}$ via $T \approx \frac{3A_{\mathrm{R}}}{2R}\frac{p}{n-1}$. The molar polarizability $A_{\mathrm{R}} = 4.195735(13)$ cm^3/mol of argon was dependent on best-knowledge of thermodynamic temperature at the gallium melting-point; consequently, the implementation is relative primary thermometry, with one key-parameter value tied to $T - T_{90}$ near 303 K. Notable aspects include a settling-time of 1500 s to reach 0.1 mK gradients, and statistical consistency of 0.5 µK/K in the multi-isotherm regression.

BACKGROUND

Refractive-index gas thermometry (RIGT) is a measurement technique that accesses thermodynamic temperature via the ideal gas law $p = \rho RT$, with p being gas pressure, ρ the molar density, R the gas constant, and T thermodynamic temperature. Because high-accuracy measurement of gas density is difficult to achieve, RIGT targets the more easily measurable quantity refractive index n as a proxy for density. Refractive index and density are related $\rho \approx \frac{2}{3A_{\mathrm{R}}}(n-1)$ via polarizability A_{R}, a fundamental optical property, and a relationship defined by the Lorentz-Lorenz equation.

An overview of refractive-index gas thermometry can be found in Ref. [1]. In simplistic terms, the one weakness of RIGT, compared to other primary thermometry methods, is that gas pressure needs to be accurately measured. Consequently, it is inconceivable that RIGT will outperform something like acoustic gas thermometry [2] in terms of absolute accuracy. Nevertheless, an optical RIGT implementation has a few things in its favor, such as the simple setup, high resolution, and compactness—and, as will be seen below, fast settling-times.

This work contributes to the ongoing international efforts [3, 4] to accurately determine $T - T_{90}$, the difference between thermodynamic temperature and the international temperature scale of 1990 (ITS-90). Knowledge of $T - T_{90}$ can be important in precision thermophysical measurement (such as thermal expansion, density virial coefficients, experimental tests of theory, etc.). Furthermore, a strong consensus on $T - T_{90}$ might one day enable a new practical temperature scale more accurate than ITS-90. In this context, RIGT is worth pursuing (as a moderately accurate technique) because it is a general principle that diverse methodologies can build a stronger consensus.

The present RIGT embodiment comprised a Fabry-Perot cavity [5] and piston-gage [6]; the cavity measured gas refractivity and the piston-gage generated the known pressure. The RIGT was compared to a best-estimate of ITS-90 via a capsule-type standard platinum resistance thermometer (cSPRT), calibrated at the fixed points of water, gallium, and indium. The apparatus builds on recent work [5]. The one refinement over Ref. [5] is the insertion of a bored copper block between the mirrors of the cavity. The arrangement is shown in Fig. 1. This critical improvement means that the cavity mode and thermometer rapidly equilibrate, as now explained.

Rapid response RIGT

The objective of this subsection is to answer the question: After the apparatus of Fig. 1 is filled with argon, how long does it take the temperature of the cSPRT to match the temperature of the cavity mode within 0.1 mK? (The "cavity mode" is the laser beam resonating between the mirrors of the cavity, as annotated in Fig. 1 and drawn as a red line. The external laser beam is aligned to the cavity mode with optics and mirrors, not shown. The "cavity" in this work

[a)]Corresponding author: egan@nist.gov

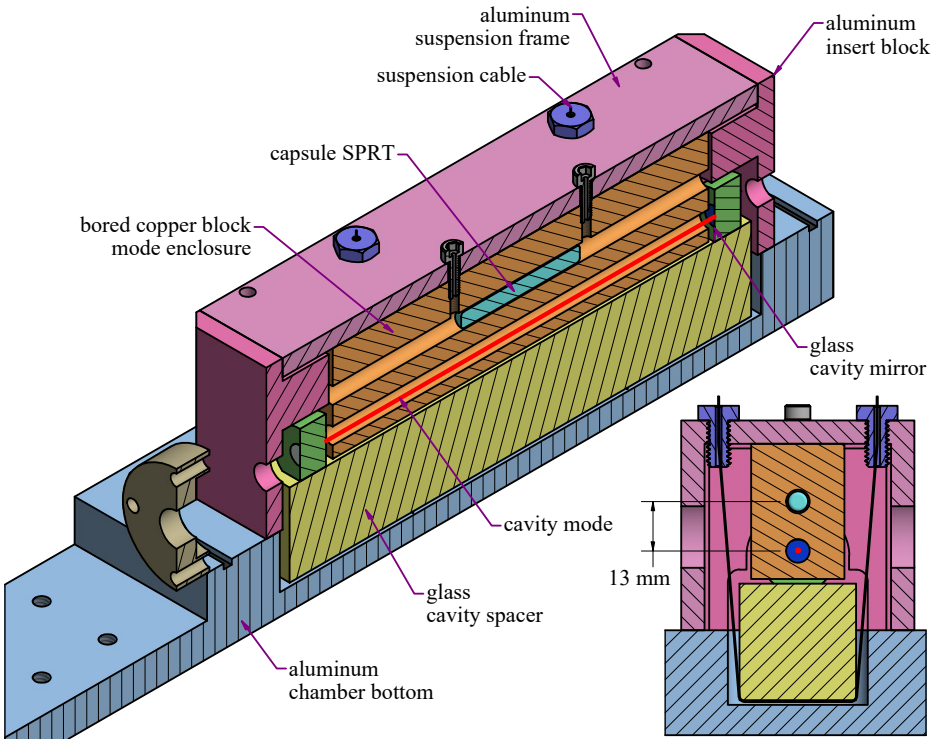

FIGURE 1. The "enclosed mode" is achieved by inserting a copper block between the mirrors of the Fabry-Perot cavity. The glass cavity is suspended by wires, free to compress/expand, and untouched by metal.

consists of two mirrors stood up on a glass spacer, also annotated in Fig. 1. This style of optical cavity does not have a hole, nor does the mode propagate in confined space. It is an "open cavity.")

The question of settling-time will be answered by a heat transfer model, which follows Ref. [7]. The gas fill is modeled as a power input to a finite-element package. The input power is the pV energy for a 36 s duration fill. The half-section gas volume of Fig. 1 is 300 mL. After the fill, heat transfers throughout the system by conduction only; there is no flow or radiative coupling. The boundary condition on the outside walls of the chamber is natural convection between parallel plates (the other plate is the inside wall of the thermal shell, not shown).

Results are shown in Fig. 2. Two representative cases are analyzed to draw contrast between settling-times. The two cases are called the "open cavity" and "enclosed mode" systems, and subplots (a) and (b) show the respective geometries and spatial gradients. The open cavity of Fig. 2(a) was how the apparatus operated in Ref. [5], in which the cavity mode propagated in an open volume of gas. The enclosed mode of Fig. 2(b) is the present implementation, in which a bored copper block has been inserted between the mirrors of the cavity, and the cavity mode propagates (mostly) inside a hole. The only geometric difference between the open cavity and the enclosed mode systems of Fig. 2(a) and (b) is that the copper block has been inserted between the cavity mirrors. Also, the finite-element model of Fig. 2(a) and (b) uses a quarter-section; the drawing of Fig. 1 is a half-section.

When the open cavity is charged to pressure, the expanding gas rapidly equilibrates with the metal walls and glass cavity. After charging the cavity is hot, and heat transfer between the cavity and the surrounding system is predominantly conduction through argon—a slow process. The cavity remains hot for a long period of time, with thermal gradients extending from the glass into the gas volume. Since the thermometer can not be placed inside the cavity mode nor provide a spatial average along the beampath, errors in temperature are inevitable. That is, the local gas temperature which the thermometer measures will invariably be different than the average gas temperature along the cavity mode. For the system of Fig. 2(a), errors in thermometry would be as large as 6.6 µK/K after 2 h of settling.

When the enclosed mode system is charged to pressure, the input energy is only 20 % smaller than the open cavity system, because some gas volume is replaced with copper. The suspended glass cavity heats up a similar amount as the open mode case. Again, gas in the vicinity of the glass is in a nonequilibrium state. However, the copper block encapsulates both the cavity mode and thermometer in a more ideal volume—high thermal effusivity. The copper

AIP Conference Proceedings 3230, doi: 10.1063/5.0234184

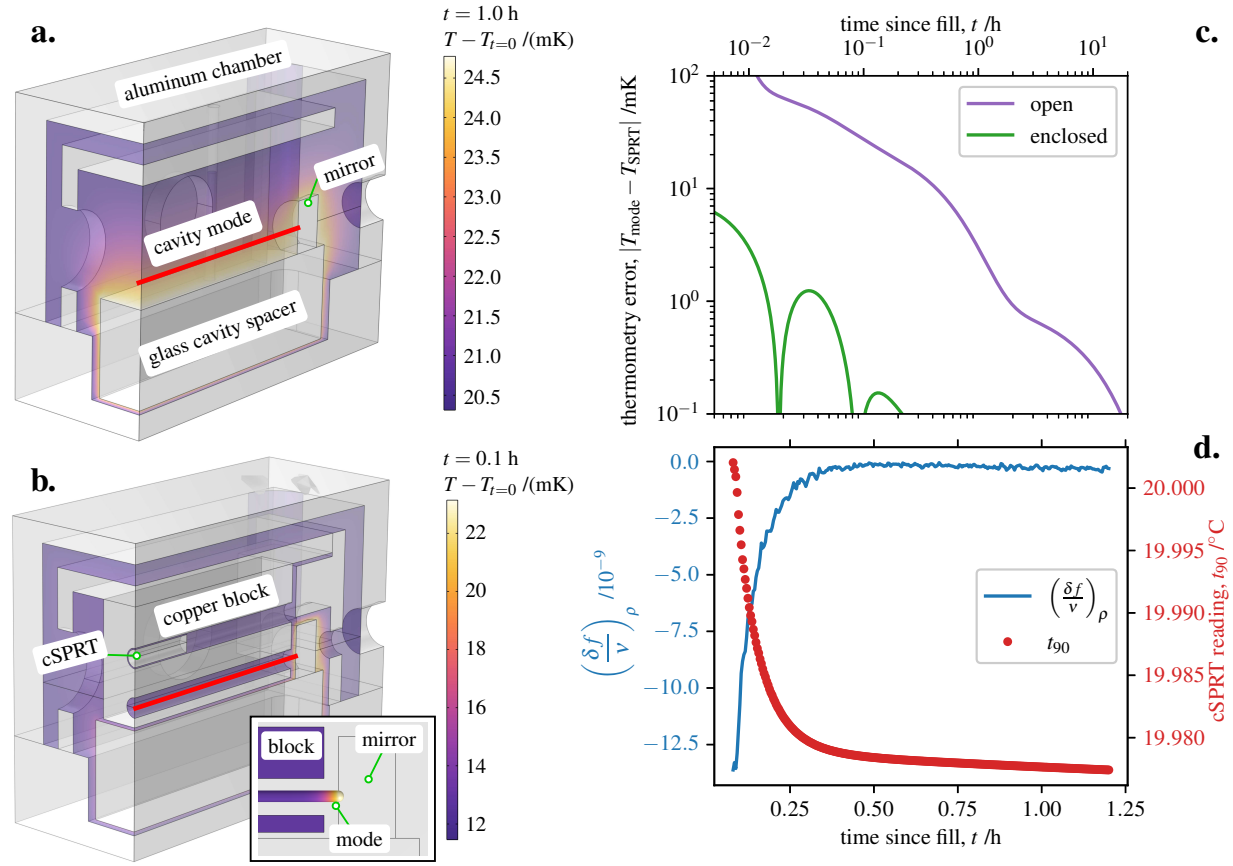

FIGURE 2. Finite-element results for temperature change in the argon volume for $\Delta p = 0.1$ MPa in the (a) open cavity and (b) enclosed mode systems. The volume contours are plotted at elapsed times of 1.0 h and 0.1 h, respectively. The inset of (b) highlights that a "hot spot" on the cavity mode exists in the clearance space between the copper block and the front of the cavity mirror. (c) Finite-element calculation of temperature gradient between the cavity mode and resistance thermometer as a function of time. (d) Experimental performance of the enclosed mode system for argon $\Delta p = 0.1$ MPa.

block effectively isolates the cavity mode and thermometer in a volume that becomes rapidly isothermal, and renders them independent of transients happening elsewhere in the system. The one flaw in this arrangement is that the copper block does not touch the cavity, and the inset to Fig. 2(b) shows that about 1 mm of the cavity mode travels through hot gas beside the mirror. After 0.1 h, the 1 mm of beampath at either mirror remains about 5 mK hotter than the copper block, which represents an error 0.07 mK of when averaged over the 150 mm cavity length.

Comparison of the simulated transient responses for the two systems is plotted in Fig. 2(c). The y-axis has T_{mode} as the average temperature of argon along a line between the center of the mirrors, and T_{SPRT} as the average temperature of a volume probe (hollow stainless steel capsule) located in the upper bore of the copper block and floating in argon. The absolute value of the thermometry error is plotted because the cSPRT in the gas volume presents a dynamic system in which the sign of the gradient fluctuates. The comparison metric of "time taken until 0.1 mK gradients" is used to compare performance. The open cavity has gradients of 0.1 mK between thermometer and cavity mode persisting for up to 15 h. The enclosed mode system has gradients less than 0.1 mK after 0.3 h. By the comparison metric of 0.1 mK gradients, the enclosed mode has reduced settling-time by a factor of 50.

Experimental validation that the cavity mode and thermometer are at the same temperature can only be done indirectly. In Fig. 2(d), the change in (cavity resonance) fractional frequency at constant density $\left(\frac{\delta f}{\nu}\right)_\rho$ is plotted over time after a $\Delta p = 0.1$ MPa charge. The pressure was generated with a piston-gage and was constant within 1 µPa/Pa, so the adjustment to constant density is predominantly a correction for the temperature change. In a perfectly stable cavity, resonant frequency at constant density would be constant as a function of time, if (and when) the thermometer accurately reflects the temperature of the cavity mode. It is evident in Fig. 2(d) that when $t > 0.4$ h, standard deviation

AIP Conference Proceedings 3230, doi: 10.1063/5.0234184

from a linear fit to $\left(\frac{\delta f}{\nu}\right)_p$ is within 5.2×10^{-11}. In terms of temperature, this fractional stability in resonant frequency corresponds to 0.2 μK/K, or 0.06 mK possible deviation between thermometer and cavity mode. This experimental observation of performance at $t > 0.4$ h is consistent with the finite-element model, which predicted errors within 0.1 mK after 0.3 h. The residual long-timescale t_{90} drift seen in Fig. 2(d) is most likely caused by slow temperature relaxation (through air) between the system Fig. 2(b) and the surrounding temperature-stabilized thermal shell (not shown). However, such a drift is much slower than the thermalization time between the between the cavity mode and the thermometer, so should not affect the results.

EXPERIMENT AND RESULTS

This work is part of an ongoing refractometry $n(p,\ t_{90})$ measurement suite of the gases helium, argon, nitrogen, ordinary water, and heavy water. Below is a synopsis of what has been achieved to date with helium and argon. These two gases provide a relative estimate of error in the temperature scale $T - T_{90}$. The approach uses helium to calibrate compressibility of the resonator, followed by argon (regressed to zero-density) to deduce thermodynamic temperature. A full description of measurement uncertainty is deferred to Ref. [8], which includes discussion of gas purity issues.

Resonator characterization

The working-equation of the refractometer

$$n - 1 = \frac{\Delta f + \kappa \Delta p \nu}{\nu(1 - \kappa \Delta p)}, \tag{1}$$

has one unknown: one-dimensional compressibility κ. The absolute resonant frequency in gas ν, and the change in pressure Δp between vacuum and gas, are measured. The change in resonant frequency Δf between vacuum and gas comprises a measured frequency difference plus a calculated multiple of the free-spectral range $\Delta\nu_{\mathrm{fsr}} \approx \frac{c}{2L(T)}$. For accurate thermometry, Δf needs a small correction for change in $\Delta\nu_{\mathrm{fsr}}$ caused by thermal expansion of the cavity length $L(T)$.

So from (1), two thermophysical properties of the resonator must be characterized: expansivity and compressibility. Expansivity is readily measured by monitoring the change in vacuum resonant frequency as a function of temperature [9]. The resonator (spacer and mirrors) of the present work is made from a low-expansion titania-silicate glass, and its thermal expansion coefficient $\alpha(T)$ is plotted in Fig. 3(a). The plotted $\alpha(T)$ is the derivative of a quartic fit to experimental measurements of fractional change in cavity length versus change in temperature. The standard deviation on residuals from the fit was 1.8×10^{-9}, corresponding to some 270 pm fluctuation in cavity length. The limit on performance is the inability to compensate for temporal drift in cavity length. Although $\alpha(T)$ of the resonator is low, it is unrealistic that the setup of Fig. 1 can infer the temperature of the glass within 2 mK. Consequently, at high temperatures, offset errors in (1) could be as large as 1.5×10^{-10}, equivalent to 60 mPa in argon pressure. Since this RIGT implementation operates $p < 0.5$ MPa, imperfect correction for resonator expansivity is a concern.

Characterizing resonator compressibility is more involved than expansivity. The compressibility was deduced

$$\kappa(T) \approx \frac{\frac{p}{T}\frac{3A_{\mathrm{R}}}{2R} - \frac{\Delta f}{\nu}}{p\left(1 + \frac{p}{T}\frac{3A_{\mathrm{R}}}{2R}\right)}, \tag{2}$$

as the difference between calculated and measured helium refractivity. Calculated refractivity $\frac{p}{T}\frac{3A_{\mathrm{R}}}{2R}$ used theoretical knowledge of polarizability A_{R} [10], the fixed value of the gas constant R, together with measurements of gas pressure p and temperature t_{90}. The measured refractivity $\frac{\Delta f}{\nu}$ was the fractional change in cavity resonant frequency, caused by the combined effects of helium gas increasing refractivity plus pressure compressing the cavity. The approximation in (2) recognizes nonlinear terms which are a consequence of refractivity being nonlinear in density, and density being nonlinear in pressure; these nonlinear terms are known from calculation [10]. The deduced compressibility of the resonator is plotted in Fig. 3(b), showing relative change as a function of temperature. The nominal value has $\kappa_{303} = 9.826 \times 10^{-12}/\mathrm{Pa}$, and the residuals from a quadratic fit have standard deviation $7.9 \times 10^{-5} \cdot \kappa_{303}$.

AIP Conference Proceedings 3230, doi: 10.1063/5.0234184

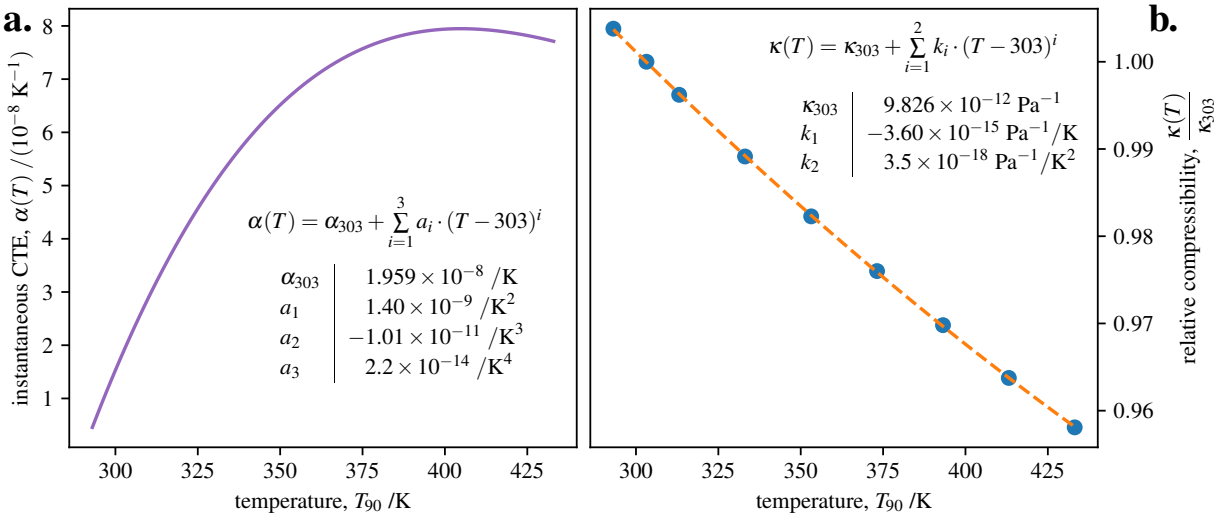

FIGURE 3. (a.) Coefficient of thermal expansion (CTE) of the resonator. (b.) Relative compressibility as a function of temperature.

Argon isotherms and $T - T_{90}$

When argon refractivity is measured at known pressure, the thermodynamic temperature is deduced by regressing

$$p = (n-1)\mathscr{A}\left[1 + (n-1)\mathscr{B} + (n-1)^2\mathscr{C}\right] + \varepsilon_p, \tag{3}$$

to recover the fit parameter $\mathscr{A} = \frac{2RT}{3A_\mathrm{R}}$ and produce T. Additional constraints are placed on the unitless coefficients $\mathscr{B}$ and $\mathscr{C}$ by multi-isotherm fitting [11]. A multi-isotherm fit is a global optimization in which the nonlinear terms of (3) follow smooth functions in temperature. In the temperature range of the present work, $\mathscr{B}(T)$ and $\mathscr{C}(T)$ are adequately described by a quartic and linear, respectively. The term ε_p in (3) allows for an offset error related to pressure, as might arise from error in force (piston-gage) or glass temperature (refractometer), mentioned above.

The fundamental quantity in (3) is the polarizability of argon A_R. The most accurate estimate of this quantity relies on knowledge of $T - T_{90}$ at an ITS-90 fixed-point [4]. Consequently, this method of RIGT is *relative primary*, and

$$\frac{T}{T^*} = \frac{\mathscr{A}}{\mathscr{A}^*} \equiv \mathscr{A}\frac{3A_\mathrm{R}}{2RT^*}, \tag{4}$$

employs "one key-parameter value determined from temperature fixed points, for which the thermodynamic temperature T is known *a priori*" [12]. The key-parameter $A_\mathrm{R} = 4.195735(13)$ cm^3/mol is established at the gallium melting-point $T^* = 302.9184(3)$ K. This measured value agrees within $5.3 \times 10^{-6} \cdot A_\mathrm{R}$ of the recommendation in Ref. [13], which adjusted an experimental measurement of the static polarizability [14] with a theoretical calculation of (sixth-order) dispersion and the magnetic susceptibility. The fit parameter $\mathscr{A}$ is unique to each isotherm, and the $\mathscr{A}$-array is produced by the multi-isotherm regression of (3). Information on thermodynamic temperatures T relative to the gallium melting-point T^* is found by the ratio of (4). Residuals on the multi-isotherm regression are shown in Fig. 4(a); the statistical estimate of uncertainty on the linear term is $(5.2 \pm 1.1) \times 10^{-7} \cdot \mathscr{A}$. For the ordinate of Fig. 4(a), the p_iso is the pressure generated by the piston gage adjusted to the average temperature isotherm, and $p(n-1)_T$ is the "optical" pressure inferred by (3)—i.e., the measurement of argon refractivity at known temperature, or, everything on the right-hand side of (3). The identified offset ε_p in Fig. 4(b) is slightly systematic at (10 ± 41) mPa, and its deviation is within reasonable estimates of the contributing causes. The dataset took 42 days to acquire by a fully-automated system in continuous operation. The dataset has 855 $n(p,\ t_{90})$ triplets: 19 set pressures repeated 5 times for each of the 9 isotherms.

The present measurements of the scale error $T - T_{90}$ are plotted in Fig. 4(c), together with the consensus estimates [3, 4] and (modern era) literature [15, 16, 17, 18, 19, 20] overlapping this range. The errorbars on "this work" are a provisional uncertainty estimate, dominated by the 1.9 µPa/Pa on pressure generated by the piston-gage [6] plus

AIP Conference Proceedings 3230, doi: 10.1063/5.0234184

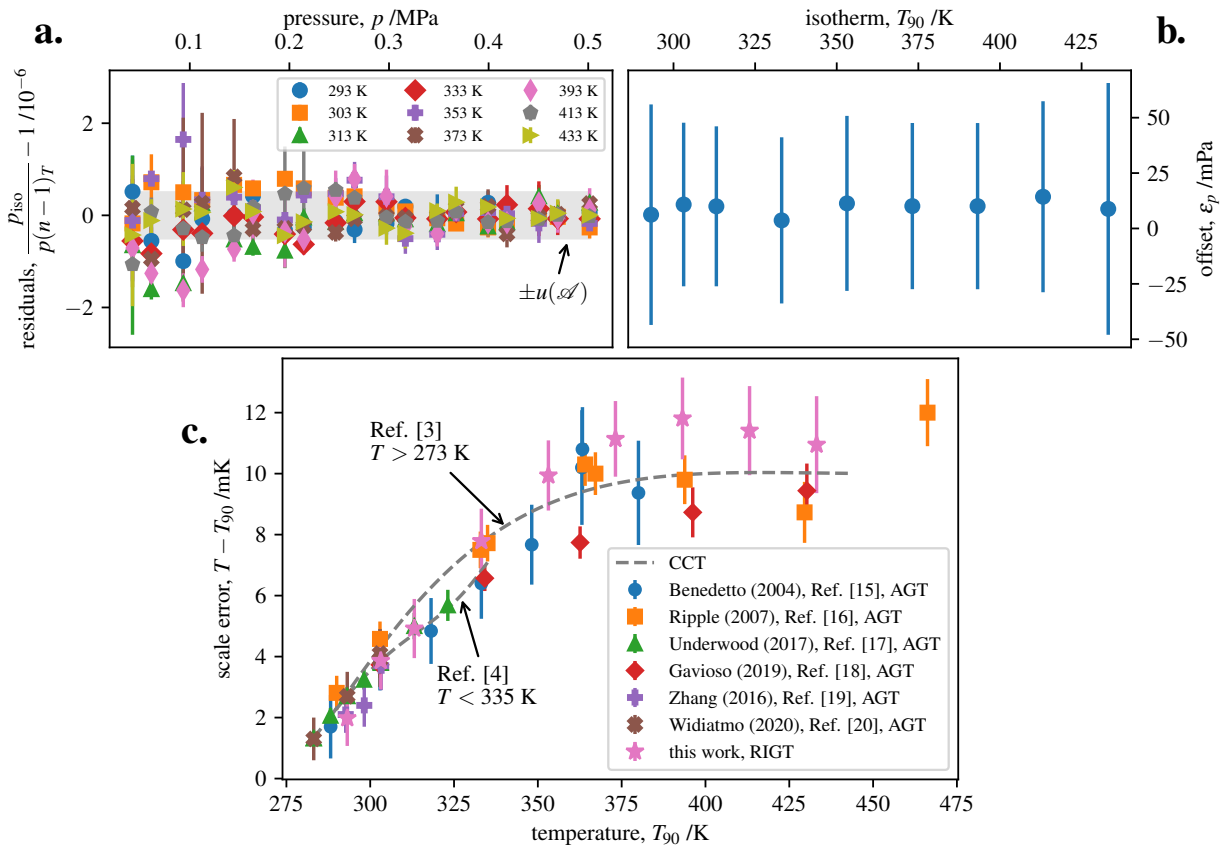

FIGURE 4. (a.) Residuals on the multi-isotherm regression of Eq. (3). Errorbars span the standard deviation on five repeats at each set pressure. (b.) Offset fit parameter identified by the multi-isotherm regression. Errorbars span the statistical estimate of standard error. (c.) Measurements of the scale error in ITS-90, with comparison to literature. Errorbars span the standard uncertainties for each reference. CCT: consultative committee for thermometry; AGT: acoustic gas thermometry.

the 1.3 µK/K reference point T^* [4]. A final evaluation will be reported in the full-length article [8]. Agreement between "this work" and the literature is good. For the three independent datapoints $T < 333$ K, agreement is middling with the new recommendation of Gaiser et al. [4]; at $T = 333$ K agreement is better with the older recommendation [3]. As $T > 380$ K, the present measurements represent only the third estimate of the scale error $T - T_{90}$ to date. Moreover, for the entire range $(293 < T < 433)$ K, the present measurements appear to be the first estimate not based on a speed of sound technique [2].

Finally for clarity, calculation of helium refractivity in (2) must use thermodynamic temperature, whereas the measured helium temperature is ITS-90. The concern here is possible circularity in T when $\kappa(T)$ is used in (1) and then later when (3) is solved for T. This concern can be allayed numerically. For example, if $T - T_{90}$ were ignored when calibrating $\kappa(T)$ with helium, the resulting error when extracting $T - T_{90}$ from the argon dataset would be no larger than 0.8 mK at 433 K. This error is two times smaller than the provisional combined uncertainty estimate $u(T - T_{90})$. Alternatively stated, this embodiment of single-cavity RIGT benefits from "pre-knowledge" of $T - T_{90}$ within 50 % at the indium freezing-point.

CONCLUSION

A working embodiment of optical RIGT has been presented, based on a Fabry–Perot cavity operating at 633 nm. From the systematic error viewpoint, the approach has much similarity with microwave resonators [1]—for both techniques, apparatus compressibility is the main error to contend with, and measurement of gas pressure is a dominant contributor

to uncertainty. However, the approach is noteworthy because of its precision and rapid settling-time. For precision, argon isotherms in the range $(293 < T < 433)$ K and $p < 0.5$ MPa have demonstrated statistical consistency at the level of 0.5 µK/K. For settling-times, the apparatus exhibits errors less than 0.1 mK between the resistance thermometer and cavity mode 1500 s after a gas charge.

Work is ongoing to complete the gas refractometry measurement suite, and detail the nonlinear terms of (3) for argon and nitrogen—functions describing $\mathscr{B}(T)$ and $\mathscr{C}(T)$ are of interest to the field of laser barometry [1, 7]. These things will be reported in a full-length article [8], together with the isotherm datasets.

REFERENCES

1. P. M. C. Rourke, "Perspective on the refractive-index gas metrology data landscape," Journal of Physical and Chemical Reference Data **50**, 033104 (2021).
2. M. R. Moldover, R. M. Gavioso, J. B. Mehl, L. Pitre, M. de Podesta, and J. T. Zhang, "Acoustic gas thermometry," Metrologia **51**, R1–R19 (2014).
3. J. Fischer, M. de Podesta, K. Hill, M. Moldover, L. Pitre, R. Rusby, P. Steur, O. Tamura, R. White, and L. Wolber, "Present estimates of the differences between thermodynamic temperatures and the ITS-90," International Journal of Thermophysics **32**, 12–25 (2011).
4. C. Gaiser, B. Fellmuth, R. M. Gavioso, M. Kalemci, V. Kytin, T. Nakano, A. Pokhodun, P. M. C. Rourke, R. Rusby, F. Sparasci, P. P. M. Steur, W. L. Tew, R. Underwood, R. White, I. Yang, and J. Zhang, "2022 update for the differences between thermodynamic temperature and ITS-90 below 335 K," Journal of Physical and Chemical Reference Data **51**, 043105 (2022).
5. P. F. Egan, "Capability of commercial trackers as compensators for the absolute refractive index of air," Precision Engineering **77**, 46–64 (2022).
6. P. F. Egan, E. S. Stanfield, J. R. Stoup, and C. W. Meyer, "Conversion of a piston–cylinder dimensional dataset to the effective area of a mechanical pressure generator," Metrologia **61**, 065004 (2024).
7. P. F. Egan, J. A. Stone, J. K. Scherschligt, and A. H. Harvey, "Measured relationship between thermodynamic pressure and refractivity for six candidate gases in laser barometry," Journal of Vacuum Science & Technology A **37**, 031603 (2019).
8. P. F. Egan and Y. Yang, "Optical $n(p, T_{90})$ measurement suite 1: He, Ar, and N_2," International Journal of Thermophysics **44**, 181 (2023).
9. S. F. Jacobs, J. N. Bradford, and J. W. Berthold, "Ultraprecise measurement of thermal coefficients of expansion," Applied Optics **9**, 2477–2480 (1970).
10. M. Puchalski, K. Piszczatowski, J. Komasa, B. Jeziorski, and K. Szalewicz, "Theoretical determination of the polarizability dispersion and the refractive index of helium," Physical Review A **93**, 032515 (2016).
11. D. Gugan, "The analysis of ^{4}He isotherms: Density and dielectric virial coefficients, and the accuracy of NPL-75," Metrologia **19**, 147–162 (1984).
12. Consultative Committee for Thermometry, "*Mise en pratique* for the definition of the kelvin in the SI," Tech. Report. (Bureau International des Poids et Mesures, 2019) SI Brochure—9th edition (2019)—Appendix 2.
13. M. Lesiuk and B. Jeziorski, "First-principles calculation of the frequency-dependent dipole polarizability of argon," Physical Review A **107**, 042805 (2023).
14. C. Gaiser and B. Fellmuth, "Polarizability of helium, neon, and argon: new perspectives for gas metrology," Physical Review Letters **120**, 123203 (2018).
15. G. Benedetto, R. M. Gavioso, R. Spagnolo, P. Marcarino, and A. Merlone, "Acoustic measurements of the thermodynamic temperature between the triple point of mercury and 380 K," Metrologia **41**, 74–98 (2004).
16. D. C. Ripple, G. F. Strouse, and M. R. Moldover, "Acoustic thermometry results from 271 to 552 K," International Journal of Thermophysics **28**, 1789–1799 (2007).
17. R. Underwood, M. de Podesta, G. Sutton, L. Stanger, R. Rusby, P. Harris, P. Morantz, and G. Machin, "Further estimates of $(T - T_{90})$ close to the triple point of water," International Journal of Thermophysics **38**, 44 (2017).
18. R. M. Gavioso, D. M. Ripa, P. P. M. Steur, R. Dematteis, and D. Imbraguglio, "Determination of the thermodynamic temperature between 236 K and 430 K from speed of sound measurements in helium," Metrologia **56**, 045006 (2019).
19. K. Zhang, X. J. Feng, J. T. Zhang, Y. Y. Duan, H. Lin, and Y. N. Duan, "Determination of $T - T_{90}$ from 234 K to 303 K by acoustic thermometry with a cylindrical resonator," Metrologia **57**, 024004 (2020).
20. J. V. Widiatmo, T. Misawa, T. Nakano, and I. Saito, "Thermodynamic temperature measurements from the triple point of water up to the melting point of gallium," International Journal of Thermophysics **41**, 42 (2020).